HHS Public Access

Author manuscript

Ann Biomed Eng. Author manuscript; available in PMC 2018 January 01.

Published in final edited form as:

Ann Biomed Eng. 2017 January ; 45(1): 261–272. doi:10.1007/s10439-016-1646-y.

Effect of chemistry on osteogenesis and angiogenesis towards bone tissue engineering using 3D printed scaffolds

Susmita Bose[*], **Solaiman Tarafder**, and **Amit Bandyopadhyay**

W. M. Keck Biomedical Materials Research Laboratory, School of Mechanical and Materials Engineering, Washington State University, Pullman, WA 99164, USA

Abstract

The functionality or survival of tissue engineering constructs depends on the adequate vascularization through oxygen transport and metabolic waste removal at the core. This study reports the presence of magnesium and silicon in 3D printed tricalcium phosphate (TCP) scaffolds promotes *in vivo* osteogenesis and angiogenesis when tested in rat distal femoral defect model. Scaffolds with three different interconnected macro pore sizes were fabricated using direct three dimensional printing (3DP). *In vitro* release in phosphate buffer for 30 days showed sustained Mg^{2+} and Si^{4+} release from these scaffolds. Histolomorphology and histomorphometric analysis from the histology tissue sections revealed a significantly higher bone, between 14 and 20 % for 4 to 16 weeks, and blood vessel, between 3 and 6% for 4 to 12 weeks, formation due to the presence of magnesium and silicon in TCP scaffolds compared to bare TCP scaffolds. The presence of magnesium in these 3DP TCP scaffolds also caused delayed TRAP activity. These results show that magnesium and silicon incorporated 3DP TCP scaffolds with multiscale porosity have huge potential for bone tissue repair and regeneration.

Keywords

Matrix mineralization; bone histomorphometry; 3D printing; calcium phosphates; osteogenesis; angiogenesis; injury/fracture healing

Introduction

Calcium phosphate (CaP) biomaterials are widely used in many clinical applications because of their compositional similarities to bone mineral, excellent biocompatibility, bioactivity and non-immunogenicity.[5,15,50,28,41] CaPs also offer the advantage of being custom manufactured with respect to the patient and target application based on the computed tomography (CT) scan of the fracture or wounded site. Tricalcium phosphate [TCP, β-$Ca_3(PO4)_2$] is one of the most attractive bioceramics among other CaPs in bone tissue engineering since it shows an excellent biocompatibility, osteoconductivity, and

[*] sbose@wsu.edu; Phone: (509) 335-7461.

Supporting Information

Part of the materials and methods, schematic of the defect model, photomicrographs of hematoxylin and eosin (H&E) stained tissue sections for early time points, and photomicrographs of TRAP staining are provided in the supporting information.

resorbability.[6,50] The resorption properties of TCP makes it degrade over time and replaced by host tissue.

Many trace elements such as Mg^{2+}, Si^{4+}, Sr^{2+}, Zn^{2+} and Na^{+} are also present in the bone mineral.[2,3,12,26,32] In many cases, cation substituted CaPs demonstrated high mechanical properties and improved biological responses as well. Cation substitution in CaPs can introduce changes in their crystallinity, microstucture and solubility. These physicochemical properties changes in CaPs bioceramics influence their mechano-biological behavior significantly. We have shown in our previous works that TCP with tunable mechanical properties can be achieved without compromising the inherent biocompatibility of TCP by appropriate cation substitution at the optimum concentration.[3,6,11,45,46] Magnesium plays a vital role in human physiology through its action as a cofactor in numerous enzymatic reactions. It stabilizes structure of proteins, nucleic acids, modulates signal transduction, and cell proliferation.[49,54] Low dietary Mg^{2+} intake showed that this cation has an effect on bone and mineral metabolism.[44] Silicon (Si^{4+}) is present in connective tissues and bone.[22] Silicon is involved in early stage bone formation through the synthesis and/or structural stabilization of collagen.[8,39] The role of silicon in bone formation has been demonstrated by its association between dietary intake and higher bone mineral density.[24]

Angiogenesis or new blood vessel formation is required for any tissue-engineered constructs to be functional. Survival of any tissue is dependent on the nutrient and oxygen supply from blood vessels.[42] Vascular ingrowth from the host tissue to the implanted compact tissue construct is very superficial. As a result, the core of the tissue-engineered construct is deprived of proper nutrient and oxygen supply, which results in the ultimate failure of the implant. Tissue engineering scaffolds with interconnected pores and multiscale porosity supports oxygen and nutrient supply to the core of the scaffold, and thus helping adequate vascularization.[20,25,47] Moreover, these type of tissue engineering scaffolds provide better mechanical interlocking between scaffold and host tissue through tissue ingrowth into interconnected macro pores.[37,38,48,56]

Fabrication of CaP scaffolds with complex architectural feature is quite challenging by conventional methods due to lack of precise control over pore size, distribution, interconnectivity, and volume fraction porosity.[1,10,50,51,52] Our earlier work with 0.5 wt. % SiO_2 and 0.25 wt. % ZnO doped 3DP TCP scaffolds[11,12] investigated both *in vitro*[12] and *in vivo*[13] performance of these scaffolds on osteoblasts cells and in a rat distal femoral defect model, respectively. Our *in vivo* work with 1 wt. % SrO and 1 wt. % MgO doped 3DP TCP scaffolds showed very promising induced bone formation caused by the presence of these dopants in TCP scaffolds in both rat[51] and rabbit[52] models.

The substantial evidence from literature and from our own work on the positive effect of Mg^{2+} and Si^{4+} on both osteogenesis and angiogenesis led us examine the effect of the coexistence of magnesium (Mg^{2+}) and silicon (Si^{4+}) in 3DP interconnected macro porous TCP scaffolds on the mechanical strength, and *in vivo* osteogenesis and angiogenesis. In addition to the effect on osteogenesis, we examined the role of these dopants on in vivo new blood vessel formation in the newly formed bone within the 3DP TCP scaffolds. None of our earlier studies examined the effect of the coexistence of Mg^{2+} and Si^{4+} on in vivo

osteogenesis and angiogenesis. We report here the influence of multiscale porosity, and the coexistence of Mg^{2+} and Si^{4+} on *in vivo* angiogenic bone regeneration in a rat distal femoral defect model for 4, 8, 12, 16 and 20 weeks.

2. Materials and Methods

2.1. Scaffold fabrication

Commercial grade β-TCP (purchased from Berkeley Advanced Biomaterials Inc., Berkeley, CA; 550 nm average particle size) was used to fabricate the pure and 0.5 wt. % MgO and 0.5 wt. % SiO_2 doped TCP scaffolds. MgO (0.5 wt. %) and SiO_2 (0.5 wt. %) percentages were chosen based on our earlier works to introduce enhanced mechanical and biological properties in the 3D printed TCP scaffolds.[6,11,12,51] Powder mixing and dryning were carried out following our previously reported procedure.[6] All scaffolds were ccylindrical in shape and had 3D interconnected square-shaped macropores. Three different pore sizes (500 mm, 750 mm and 1000 mm) for mechanical strength analysis, and only one pore size (350 μm) for *in vivo* implantation were fabricated using a 3D printer (ProMetal®, ExOne LLC, Irwin, PA, USA). The dimension of scaffolds for mechanical testing and in vivo implantation were 7 mm (dia) x 10.5 mm (height) and 3.4 mm (dia) x 5.2 mm (height), respectively. Figure 1(a) presents a 3D printing process schematic. The 3DP process description can be found in the supporting information.

2.2. Microstructure, phase, pore size, porosity, and mechanical strength analysis

X-ray diffraction (XRD) patterns were used for phase analysis of the sintered scaffolds. Volume fraction porosity was determined from the apparent and the bulk densities. Scanning electron microscope (SEM) images were used for pore size measurement and surface morphologies of sintered scaffolds. Compressive strength of the scaffolds was determined using a screw-driven universal testing machine (AG-IS, Shimadzu, Tokyo, Japan) with a constant crosshead speed of 0.33 mm/min (n = 10 for each composition).

2.3. Surgery and implantation procedure

Rat bone defect is an excellent model to be used for proof-of-concept study in a laboratory set up, which is widely reported in literature for fair assessment of bone biology and remodeling during fracture healing. A total 20 male rats (Sprague-Dawley rats with average body weight of 300 g were purchased from Simonsen Laboratories, Gilroy, CA, USA), four rats (n=4, chosen randomly) at each time points, were used. Following acclimatization, all rats received a control implant in the right and a doped implant in the left distal femur through a 3 mm diameter cortical defect surgery using a 3 mm drill bit. The rats had free access to food and water in a temperature and humidity controlled room with 12-hour cycles of light and dark, and two rats were housed together in one cage. IsoFlo® (isoflurane, USP, Abbott Laboratories, North Chicago, IL, USA) coupled with an oxygen (Oxygen USP, A-L Compressed Gases Inc., Spokane, WA, USA) regulator were used to anesthetize the rats. Rats were euthanized at predetermined time points by halothane overdose followed by 70% potassium chloride intracardiac injection. Animal experimental protocol was approved by the Washington State University Institutional Animal Care and Use Committee (IACUC).

2.3.1. Histomorphology—A 10% buffered formalin solution was used for 72 h as fixative to fix the bone-scaffold specimens. The formaline fixed specimens were then processed further for either undecalcified or decalcified tissue sections preparation.

2.3.1.1. Hematoxylin and eosin (H&E) staining: Decalcification was carried out by keeping the formaline fixed bone-implant specimens in 14 % ethylenediaminetetraacetic acid (EDTA). Once decalcification was completete, samples were dehydrated, embedded in paraffin, and cut into thin tissue sections (5 to 10 μm thick) using a microtome. These tissue sections were deparaffined, hydrated and stained using hematoxylin and eosin (H&E).

2.3.1.2. Tartrate resistant acis phosphatase (TRAP) staining: A previously published procedure[19] was followed for TRAP staining. Briefly, deparaffined tissue sections were incubated for 30 min at 37 °C in preheated sodium acetate buffer of pH 4.9 with naphthal AS-BI phosphate (Sigma). The slides were then incubated for 5 min at room temperature in a filtered pararosanilline and sodium nitrate. Finally, the slides were rinsed with distilled water, counterstained for 30 sec in hematoxylin, dehydrated, and mounted.

2.3.1.3. Blood vessel staining: von Willebrand Factor (vWF) is an endothelial cell markers for angiogenesis. Thus, vWF labelled cells would detect angiogenesis. Deparaffinized histology slides were stained for vWF using a blood vessel staining kit (ECM590, Millipore, MA, USA) per the manufacturer's instructions. Rabbit anti-vWF polyclonal antibody supplied in the kit was used as the primary anibody. Aantigen retrieval was carried out by heating the the slides in a vegetable steamer for 20 min in sodium citrate buffer (10mM Sodium Citrate, 0.05% Tween 20, pH 6.0) was used. Stained tissue sections were counterstained by hematoxylin followed by dehydration.

2.3.2. Histomorphometric analysis—H&E, TRAP, and vWF stained tissue sections were used for new bone area (bone area/area of the entire tissue section, %), TRAP activity (TRAP positive area/area of the entire tissue section, %), and blood vessel area (blood vessel area/total area, %) analysis, respectively. A freely available software (Image J, National Institute of Health) was used for this purpose. Bone area and TRAP activity were measured from 800 μm width and 800 μm height tissue sections (n = 8), whereas blood vessel area was measured from 200 μm width and 200 μm height tissue sections (n = 8).

2.4. Mg^{2+} and Si^{4+} ions release

To investigate the ion Mg^{2+} and Si^{4+} ions release behavior from Mg-Si doped 3DP TCP scaffolds, samples were immeresed into pH 7.4 phosphate buffer saline and kept at 37 °C for 30 days under 150 RPM. Buffer media was changed at specific time intervals. Buffer solution was replaced at each time point with fresh solution. Analysis of Mg^{2+} and Si^{4+} ions concentration in the release media was carried out using a Shimadzu AA-6800 atomic absorption spectrophotometer (AAS) (Shimadzu, Kyoto, Japan).

Data are presented as mean ± standard deviation where appropriate. Statistical analysis was performed using student's t-test on bone area, blood vessel area and TRAP activity. A P value < 0.05 was considered significant.

3. Results

3.1. Phase, microstructure, porosity and mechanical properties

Figure 1(b) shows sintered 0.5 wt. % MgO and 0.5 wt. % SiO_2 doped TCP scaffolds, and Figure 1(c) presents the XRD spectra of the scaffolds along with the as received TCP powder for comparison purpose. Peaks for both β-TCP (JCPDS # 09-0169) and α-TCP (JCPDS # 09-0348) were observed in sintered pure TCP scaffolds. The occurrence of some α-TCP peaks were due to high temperature phase transformation from β to α. Any β to α phase transformation was not observed in MgO-SiO_2 doped TCP. Large number of intrinsic and residual micro pores (20 μm or less in size) were seen on the both pure and doped scaffold struts as can be viewed from the surface morphology as presented in Figure 2. A comparison between designed and sintered pore size and porosity is presented in Table 1. Sintered pore size was always smaller than the designed pore size due to the high temperature densification process during sintering. A higher total porosity was always exhibited by the sintered scaffolds compared to designed porosity because of the intrinsic and residual micro pores. Size of the pores has a significant role on vascularization and tissue in-growth into the tissue engineering constructs. Although the suggested minimum effective pore size for bone tissue formation through adequate transport of oxygen and nutrients for the survivability of the cells is 100 μm,[18,43] interconnected macro pores between 200–350 μm are highly recommended for successful vascularized tissue formation.[33] Therefore, we designed scaffolds with 350 μm interconnected macro pores for *in vivo* implantation, which resulted in 268 ± 9.8 μm and 311 ± 5.9 μm [2] for doped and pure TCP scaffolds, respectively. Table 1 also shows how the presence of these dopants (Mg^{2+} as MgO and Si^{4+} as SiO_2) affected compressive strength, where the values for the pure TCP scaffolds are provided from our previous study[50] for comparison purpose. MgO and SiO_2 addition in pure TCP caused insignificant increase in compressive strength. This indicates that addition of MgO and SiO_2 in TCP did not deteriorate its mechanical strength. A maximum compressive strength of 6.79 ± 1.14 MPa was observed for the 500 μm MgO-SiO_2 doped scaffolds.

3.2. Histomorphology, Histomorphometric analysis, and Mg^{2+} and Si^{4+} ions release

The schematic of the defect model is presented in Figure S1 (provided in the Supporting Information). Induced bone formation by pure and Mg-Si doped TCP was observed by H&E staining as presented in Figure 3(a) for 16 and 20 weeks, where newly formed bone can be seen inside the micro and macro pores. Early time points (4, 8 and12 weeks) H&E stained tissue sections can be seen in the Figure S2. Acellular zones in the figure are resulted from the demineralization process. Figure 3(b) shows quantification of new bone formation through histomorphometric analysis of new bone area calculated from H&E stained tissue sections. Figure 3(b) exhibits that MgO and SiO_2 induced new bone formation, between 14 and 20%, at early time points for 4 to 16 weeks. Although the difference between pure and doped scaffolds was low at 20 weeks, ~ 5% higher in doped TCP, but it was significant.

Figure S3 shows the positive activity of TRAP positive cells at each time point inside all pure and doped TCP scaffolds suggesting bone resorbing osteoclasts activity. Figure 4 presents histomorphometric comparison of TRAP positive cells activity between pure and

doped TCP. A significantly higher TRAP positive cells activity, ~ 6 and 3%, was observed in pure TCP after 4 and 12 weeks. Doped TCP scaffolds induced higher TRAP activity, ~ 4 and 3%, after 8 and 16 weeks compared to pure TCP. No significant difference in TRAP activity was observed after 20 weeks.

Formation of new tissue and its functionality is very much dictated by new blood vessel formation. Figure 5 shows blood vessel formation inside both pure and Mg-Si doped TCP scaffolds after 4, 8 and 12 weeks. These TCP scaffolds induced new blood vessel formation. Nevertheless, an increase in blood vessel formation, between 3 and 6%, was observed in Mg-Si-TCP compared to pure TCP scaffolds. Figure 6a presents histomorphometric comparison of blood vessel area. The comparison between blood vessel area shows Mg-Si-TCP induced significantly higher blood vessel formation at early time points compared to its pure counterpart. This indicates the beneficial effect of MgO and SiO_2 in TCP for angiogenesis at the early stage of wound healing. Figure 6b and c presents the cumulative ions (Mg^{2+} and Si^{4+}) release from the Mg-Si doped TCP scaffolds. A much higher *in vitro* Si^{4+} ions release than Mg^{2+} ions were observed from these Mg-Si doped scaffolds.

Discussion

The three dimensional printing (3DP) offers a great advantage of direct scaffold fabrication from CaP based bioceramic powder with the ability of making patient-specific bone graft substitutes from computed tomography data.[9] In our earlier studies, we examined the effect of binary doping on *in vivo* osteogenesis and angiogenesis in rat[13,51] and rabbit[52] models: (i) 1 wt.% SrO & 1 wt.% MgO[51,52] and (ii) 0.5 wt.% SiO2 & 0.25 wt.% ZnO[13] doped 3DP TCP scaffold. Multiscale porosity is a great feature of these scaffolds, which is exhibited by the presence of intrinsic micro pores along with the designed macro pores as shown in Figure 2. These intrinsic micro pores are the reason for the difference between designed and sintered porosity (as presented in Table 1). The absence of any compaction process during 3DP direct scaffold fabrication resulted in the existence of these intrinsic micro pores.[50] Tissue engineering scaffolds having multiscale porosity along with a 3D interconnected microenvironment facilitate increased overall performance through enhanced osteoconduction and osseointegration.[16,17,29]

Microstructure, phase stability, mechanical properties, and strength degradation kinetics of β-TCP are greatly influenced by the dopants. Stable β-TCP can be obtained at temperatures up to 1125 °C, whereas the stable α-TCP phase beyond 1125 °C maintains its stablity up to 1430 °C.[35] The β-TCP resulted in around 25% α-TCP and 75% β-TCP, when sintered at 1250 °C for 2 h.[50] The disappearance of α-TCP phase in MgO-SiO_2-TCP scaffolds at 1250 °C sintering temperature indicates β phase stabilization due to Mg^{2+} addition, which is in line with our other reported results.[3,6,50] Replacement of Ca^{2+}(ionic radius 0.99 Å) by Mg^{2+} (ionic radius 0.69 Å) results in a reduced unit cell of the β-TCP lattice. Si^{4+} (ionic radius 2.71 Å) is substituted for P^{5+} (ionic radius 1.28 Å) instead of Ca^{2+} in the crystal lattice of TCP. The additional stability of the crystal lattice caused by the presence of Mg^{2+} ions retards dissolution of CaP, while Si^{4+} substitution for P^{5+} introduces crystal defect in the lattice and causes an increase in the solubility of TCP.[6,36] This defect caused by Si^{4+} substitution might have also led some SiO_2 or silicon substituted CaP reach area in the grain

boundary region,[6,14] which explains higher Si^{4+} ions release observed in this study. However, the co-existence of Mg^{2+} and Si^{4+} in TCP minimizes the effects caused by each other to some extent, thus the strength of the Mg-Si-TCP scaffolds remained similar as that of pure TCP scaffolds.

$MgO\text{-}SiO_2$ doping in TCP clearly indicates their effect on early wound healing through accelerated new bone tissue formation as shown in Figure 3(a). Interconnected multiscale porosity facilitated the osteoprogenitor cells penetration resulting in new bone formation in these TCP scaffolds. Osteogenic tissue scaffolds facilitate osteoprogenitor cells recruitment to the injury or wounded site. Increased new bone formation, between 14 and 20 % for 4 to 16 weeks and ~ 5% at 20 weeks, was observed over time in Mg-Si-TCP compared to its pure counterpart. This can be interpreted that Mg^{2+} and Si^{4+} when added in TCP might have facilitated the recruitment of osteoprogenitor cells resulting in accelerated bone formation, which was further substantiated by the significant difference in new bone area between doped and pure TCP as presented by the quantitative histomorphometric analysis in Figure 3(b). Our earlier studies showed that the presence of magnesium in CaP bioceramics can induce increased cellular adhesion, proliferation and alkaline phosphatase (ALP) production by osteoblasts cells [9][46]. Magnesium doped CaPs showed enhanced osteogenesis by inducing bone formation in both animal (rabbit) and human, respectively [47][48][49]. Silicon (Si^{4+}) has been shown to have stimulatory effect on proliferation and osteogenic differentiation and mineralization of both osteoblast-like bone forming cells and mesenchymal stem cells.[4,21,40] Si^{4+} is known to have a vital role in the synthesis and/or stabilization of collagen, which is believed to cause early stage bone regeneration by silicon.[23,40]

Bone resorbing osteoclast cells secrete TRAP as the principal acid during bone resorption.[53] Both pure and doped scaffolds showed TRAP positive cells activity by TRAP staining of the decalcified tissue sections (Figure S3). The maximum TRAP activity was observed at 4 weeks for pure, and the minimum at 20 weeks for both pure and doped TCP (Figure 4). Higher TRAP activity at later time points (8 and 16 weeks) in doped TCP is probably caused by the presence of Mg^{2+}. In a different study, we have shown that the presence of Mg^{2+} in TCP slows down the osteoclasts mediated resorption process.[43] Bone resorption by osteoclasts and new bone synthesis by osteoblasts is a dynamic process of bone remodeling. Thus, the balance between these resorption and formation was catalyzed by the presence of Mg^{2+} in doped scaffolds resulted in increased bone formation.

vWF (Von Willebrand factor) is a protein that is present in the basement membranes of blood vessel.[34] Therefore, vWF positive signals in the newly formed bone tissue inside the scaffold indicate new blood vessels formation, a process known as angiogenesis. Having interconnected pores in tissue engineering scaffolds facilitates nutrient and metabolic waste transport at the scaffold core, which is vital for successful regeneration of vascularized tissue.[20,47,50] Notable blood vessel formation in both pure and doped TCP (Figure 5) is caused by the presence of multiscale porosity. Histomorphometric analysis (Figure 6a) revealed the presence of $Mg^{2+}$and Si^{4+} in TCP induced significantly higher blood vessel area formation at early time points, between 3 and 6% higher, compared to pure TCP. It has been shown that silicon (Si^{4+}) can facilitate increased blood vessel formation through

induced VEFG expression, which upregulates nitric oxide synthase and nitric oxide production in human endothelial cells [49][56]. The role of magnesium (Mg^{2+}) in angiogenesis is believed to be caused by nitric oxide production in endothelial cells.[4,30] *In vitro* continued release of Mg^{2+} and Si^{4+} from the doped scaffolds (Figure 6b and c) further shows the possibility of the presence of these ions in the *in vivo* microenvironment to exert their positive effects on both osteogenesis and angiogenesis. Figure 7 depicts the role of Mg2+ and Si4+ as dopants and multiscale porosity in 3D printed TCP scaffolds for vascularised bone tissue formation.

This study exhibits the benefits of MgO and SiO_2 doping in 3DP TCP scaffolds with multiscale porosity. Our results demonstrated 3DP TCP scaffolds with interconnected macro pores can be made to facilitated nutrient transport and adequate cell migration to the core of the scaffolds. Furtheremore, the presence of Mg^{2+} and Si^{4+} in these scaffolds promoted Mg^{2+} and Si^{4+} induced enhanced vascularized new bone tissue formation at the defect site.

Conclusion

The incorporation of magnesium and silicon in 3DP TCP scaffolds did not show any adverse effect on the mechanical strength. The presence of these trace elements in TCP was beneficial for early wound healing, which was observed by accelerated bone formation. Delayed TRAP activity was observed in magnesium and silicon incorporated TCP scaffolds due to the presence of Mg^{2+}. Pore interconnectivity and multiscale porosity in these 3DP TCP scaffolds facilitated angiogenesis. However, significantly increased blood vessel formation was observed when these trace elements, magnesium and silicon, were incorporated in TCP compared to its pure counterpart. Thus, interconnected macro porous 3DP TCP scaffolds with magnesium and silicon could be excellent candidates for early wound healing and tissue regeneration applications in bone tissue engineering.

Supplementary Material

Refer to Web version on PubMed Central for supplementary material.

Acknowledgments

We thank Valerie Lynch-Holm and Christine Davitt from Franceschi Microscopy and Imaging Center at Washington State University for their technical assistance with histology and immunohistochemistry. The authors also thank Prof. Neal M. Davies for allowing the authors to use his lab for *in vivo* study.

Funding Source

National Institutes of Health, NIBIB (Grant # NIH-R01-EB-007351).

References

1. Atala A, Kasper FK, Mikos AG. Engineering Complex Tissues. Sci Transl Med. 2012; 4:160rv12–160rv12.
2. Bandyopadhyay A, Bernard S, Xue W, Bose S. Calcium Phosphate-Based Resorbable Ceramics: Influence of MgO, ZnO, and SiO2 Dopants. J Am Ceram Soc. 2006; 89:2675–2688.

3. Banerjee SS, Tarafder S, Davies NM, Bandyopadhyay A, Bose S. Understanding the influence of MgO and SrO binary doping on the mechanical and biological properties of b-TCP ceramics. Acta Biomater. 2010; 6:4167–4174. [PubMed: 20493283]
4. Bose S, Fielding G, Tarafder S, Bandyopadhyay A. Understanding of dopant-induced osteogenesis and angiogenesis in calcium phosphate ceramics. Trends Biotechnol. 2013; 31:594–605. [PubMed: 24012308]
5. Bose S, Tarafder S. Calcium phosphate ceramic systems in growth factor and drug delivery for bone tissue engineering: A review. Acta Biomater. 2012; 8:1401–1421. [PubMed: 22127225]
6. Bose S, Tarafder S, Banerjee SS, Davies NM, Bandyopadhyay A. Understanding in vivo response and mechanical property variation in MgO, SrO and SiO2 doped β-TCP. Bone. 2011; 48:1282–1290. [PubMed: 21419884]
7. Canullo L, Heinemann F, Gedrange T, Biffar R, Kunert-Keil C. Histological evaluation at different times after augmentation of extraction sites grafted with a magnesium-enriched hydroxyapatite: double-blinded randomized controlled trial. Clin Oral Implan Res. 2013; 24:398–406.
8. Carlisle EM. Silicon: A requirement in bone formation independent of vitamin D1. Calcif Tissue Int. 1981; 33:27–34. [PubMed: 6257332]
9. Castilho M, Moseke C, Ewald A, Gbureck U, Groll J, Pires I, Teßmar J, Vorndran E. Direct 3D powder printing of biphasic calcium phosphate scaffolds for substitution of complex bone defects. Biofabrication. 2014; 6:015006. [PubMed: 24429776]
10. Derby B. Printing and Prototyping of Tissues and Scaffolds. Science. 2012; 338:921–926. [PubMed: 23161993]
11. Dhal J, Fielding G, Bose S, Bandyopadhyay A. Understanding bioactivity and polarizability of hydroxyapatite doped with tungsten. J Biomed Mater Res Part B. 2012; 100B:1836–1845.
12. Fielding GA, Bandyopadhyay A, Bose S. Effects of silica and zinc oxide doping on mechanical and biological properties of 3D printed tricalcium phosphate tissue engineering scaffolds. Dent Mater. 2012; 28:113–122. [PubMed: 22047943]
13. Fielding G, Bose S. SiO2 and ZnO dopants in three-dimensionally printed tricalcium phosphate bone tissue engineering scaffolds enhance osteogenesis and angiogenesis in vivo. Acta Biomater. 2013; 9:9137–9148. [PubMed: 23871941]
14. Gavrilov KL, Bennison SJ, Mikeska KR, Levi-Setti R. Grain boundary chemistry of alumina by high-resolution imaging SIMS. Acta Mater. 1999; 47:4031–4039.
15. de Groot, K. Bioceramics of calcium phosphate. CRC Press; 1983. p. 160
16. Habibovic P, Yuan H, van der Valk CM, Meijer G, van Blitterswijk CA, de Groot K. 3D microenvironment as essential element for osteoinduction by biomaterials. Biomaterials. 2005; 26:3565–3575. [PubMed: 15621247]
17. Hing KA, Annaz B, Saeed S, Revell PA, Buckland T. Microporosity enhances bioactivity of synthetic bone graft substitutes. J Mater Sci: Mater Med. 2005; 16:467–475. [PubMed: 15875258]
18. Hulbert SF, Young FA, Mathews RS, Klawitter JJ, Talbert CD, Stelling FH. Potential of ceramic materials as permanently implantable skeletal prostheses. J Biomed Mater Res. 1970; 4:433–456. [PubMed: 5469185]
19. Jiang X, Kalajzic Z, Maye P, Braut A, Bellizzi J, Mina M, Rowe DW. Histological Analysis of GFP Expression in Murine Bone. J Histochem Cytochem. 2005; 53:593–602. [PubMed: 15872052]
20. Jones AC, Arns CH, Hutmacher DW, Milthorpe BK, Sheppard AP, Knackstedt MA. The correlation of pore morphology, interconnectivity and physical properties of 3D ceramic scaffolds with bone ingrowth. Biomaterials. 2009; 30:1440–1451. [PubMed: 19091398]
21. Jones JR, Tsigkou O, Coates EE, Stevens MM, Polak JM, Hench LL. Extracellular matrix formation and mineralization on a phosphate-free porous bioactive glass scaffold using primary human osteoblast (HOB) cells. Biomaterials. 2007; 28:1653–1663. [PubMed: 17175022]
22. Jugdaohsingh R. SILICON AND BONE HEALTH. J Nutr Health Aging. 2007; 11:99. [PubMed: 17435952]
23. Jugdaohsingh R, Calomme MR, Robinson K, Nielsen F, Anderson SHC, D'Haese P, Geusens P, Loveridge N, Thompson RPH, Powell JJ. Increased longitudinal growth in rats on a silicon-depleted diet. Bone. 2008; 43:596–606. [PubMed: 18550464]

24. Jugdaohsingh R, Tucker KL, Qiao N, Cupples LA, Kiel DP, Powell JJ. Dietary Silicon Intake Is Positively Associated With Bone Mineral Density in Men and Premenopausal Women of the Framingham Offspring Cohort. J Bone Miner Res. 2004; 19:297–307. [PubMed: 14969400]
25. Karageorgiou V, Kaplan D. Porosity of 3D biomaterial scaffolds and osteogenesis. Biomaterials. 2005; 26:5474–5491. [PubMed: 15860204]
26. Lakhkar NJ, Lee I-H, Kim H-W, Salih V, Wall IB, Knowles JC. Bone formation controlled by biologically relevant inorganic ions: Role and controlled delivery from phosphate-based glasses. Adv Drug Deliv Rev. 2013; 65:405–420. [PubMed: 22664230]
27. Landi E, Logroscino G, Proietti L, Tampieri A, Sandri M, Sprio S. Biomimetic Mg-substituted hydroxyapatite: from synthesis to in vivo behaviour. J Mater Sci: Mater Med. 2008; 19:239–247. [PubMed: 17597369]
28. LeGeros RZ. Calcium Phosphate-Based Osteoinductive Materials. Chem Rev. 2008; 108:4742–4753. [PubMed: 19006399]
29. Lan Levengood SK, Polak SJ, Wheeler MB, Maki AJ, Clark SG, Jamison RD, Wagoner Johnson AJ. Multiscale osteointegration as a new paradigm for the design of calcium phosphate scaffolds for bone regeneration. Biomaterials. 2010; 31:3552–3563. [PubMed: 20153042]
30. Li H, Chang J. Bioactive silicate materials stimulate angiogenesis in fibroblast and endothelial cell co-culture system through paracrine effect. Acta Biomater. 2013; 9:6981–6991. [PubMed: 23416471]
31. Maier JA, Bernardini D, Rayssiguier Y, Mazur A. High concentrations of magnesium modulate vascular endothelial cell behaviour in vitro. BBA-Mol Basis Dis. 2004; 1689:6–12.
32. Mouriño V, Cattalini JP, Boccaccini AR. Metallic ions as therapeutic agents in tissue engineering scaffolds: an overview of their biological applications and strategies for new developments. J R Soc Interface. 2012; 9:401–419. [PubMed: 22158843]
33. Murphy CM, Haugh MG, O'Brien FJ. The effect of mean pore size on cell attachment, proliferation and migration in collagen–glycosaminoglycan scaffolds for bone tissue engineering. Biomaterials. 2010; 31:461–466. [PubMed: 19819008]
34. Murphy WL, Simmons CA, Kaigler D, Mooney DJ. Bone Regeneration via a Mineral Substrate and Induced Angiogenesis. J Dent Res. 2004; 83:204–210. [PubMed: 14981120]
35. Perera FH, Martínez-Vázquez FJ, Miranda P, Ortiz AL, Pajares A. Clarifying the effect of sintering conditions on the microstructure and mechanical properties of [beta]-tricalcium phosphate. Ceram Int. 2010; 36:1929–1935.
36. Pietak AM, Reid JW, Stott MJ, Sayer M. Silicon substitution in the calcium phosphate bioceramics. Biomaterials. 2007; 28:4023–4032. [PubMed: 17544500]
37. Qi QQ, Chen JD, Gao SZ, Bu J, Qiu ZP. Preparation Cell Scaffolds with Well Defined Pore Structure Through Elastic Porogen/Pressure Filtration. Adv Mater Res. 2011; 236–238:1897–1901.
38. Ramay HRR, Zhang M. Biphasic calcium phosphate nanocomposite porous scaffolds for load-bearing bone tissue engineering. Biomaterials. 2004; 25:5171–5180. [PubMed: 15109841]
39. Reffitt D, Ogston N, Jugdaohsingh R, Cheung HF, Evans BA, Thompson RP, Powell J, Hampson G. Orthosilicic acid stimulates collagen type 1 synthesis and osteoblastic differentiation in human osteoblast-like cells in vitro. Bone. 2003; 32:127–135. [PubMed: 12633784]
40. Reffitt D, Ogston N, Jugdaohsingh R, Cheung HF, Evans BA, Thompson RP, Powell J, Hampson G. Orthosilicic acid stimulates collagen type 1 synthesis and osteoblastic differentiation in human osteoblast-like cells in vitro. Bone. 2003; 32:127–135. [PubMed: 12633784]
41. Rey C. Calcium phosphate biomaterials and bone mineral. Differences in composition, structures and properties. Biomaterials. 1990; 11:13–15.
42. Rouwkema J, Rivron NC, van Blitterswijk CA. Vascularization in tissue engineering. Trends Biotechnol. 2008; 26:434–441. [PubMed: 18585808]
43. Roy M, Bose S. Osteoclastogenesis and osteoclastic resorption of tricalcium phosphate: Effect of strontium and magnesium doping. J Biomed Mater Res Part A. 2012; 100A:2450–2461.
44. Rude RK, Gruber HE, Norton HJ, Wei LY, Frausto A, Kilburn J. Dietary magnesium reduction to 25% of nutrient requirement disrupts bone and mineral metabolism in the rat. Bone. 2005; 37:211–219. [PubMed: 15923157]

45. Seeley Z, Bandyopadhyay A, Bose S. Influence of TiO2 and Ag2O addition on tricalcium phosphate ceramics. J Biomed Mater Res Part A. 2007; 82:113–121.
46. Seeley Z, Bandyopadhyay A, Bose S. Tricalcium phosphate based resorbable ceramics: Influence of NaF and CaO addition. Mater Sci Eng: C. 2008; 28:11–17.
47. Seyednejad H, Gawlitta D, Kuiper RV, de Bruin A, van Nostrum CF, Vermonden T, Dhert WJA, Hennink WE. In vivo biocompatibility and biodegradation of 3D-printed porous scaffolds based on a hydroxyl-functionalized poly(ε-caprolactone). Biomaterials. 2012; 33:4309–4318. [PubMed: 22436798]
48. Sicchieri LG, Crippa GE, de Oliveira PT, Beloti MM, Rosa AL. Pore size regulates cell and tissue interactions with PLGA-CaP scaffolds used for bone engineering. J Tissue Eng Regen Med. 2012; 6:155–162. [PubMed: 21446054]
49. Staiger MP, Pietak AM, Huadmai J, Dias G. Magnesium and its alloys as orthopedic biomaterials: A review. Biomaterials. 2006; 27:1728–1734. [PubMed: 16246414]
50. Tarafder S V, Balla K, Davies NM, Bandyopadhyay A, Bose S. Microwave-sintered 3D printed tricalcium phosphate scaffolds for bone tissue engineering. J Tissue Eng Regen Med. 2013; 7:631–641. [PubMed: 22396130]
51. Tarafder S, Davies NM, Bandyopadhyay A, Bose S. 3D printed tricalcium phosphate bone tissue engineering scaffolds: effect of SrO and MgO doping on in vivo osteogenesis in a rat distal femoral defect model. Biomater Sci. 2013; 1:1250–1259. [PubMed: 24729867]
52. Tarafder S, Dernell WS, Bandyopadhyay A, Bose S. SrO- and MgO-doped microwave sintered 3D printed tricalcium phosphate scaffolds: Mechanical properties and in vivo osteogenesis in a rabbit model. J Biomed Mater Res Part B. 2015; 103:679–690.
53. Webster TJ, Ergun C, Doremus RH, Siegel RW, Bizios R. Enhanced osteoclast-like cell functions on nanophase ceramics. Biomaterials. 2001; 22:1327–1333. [PubMed: 11336305]
54. Wu F, Su J, Wei J, Guo H, Liu C. Injectable bioactive calcium–magnesium phosphate cement for bone regeneration. Biomed Mater. 2008; 3:044105. [PubMed: 19029607]
55. Xue W, Dahlquist K, Banerjee A, Bandyopadhyay A, Bose S. Synthesis and characterization of tricalcium phosphate with Zn and Mg based dopants. J Mater Sci: Mater Med. 2008; 19:2669–2677. [PubMed: 18270806]
56. Yang S, Leong KF, Du Z, Chua CK. The Design of Scaffolds for Use in Tissue Engineering. Part II. Rapid Prototyping Techniques. Tissue Eng. 2002; 8:1–11. [PubMed: 11886649]

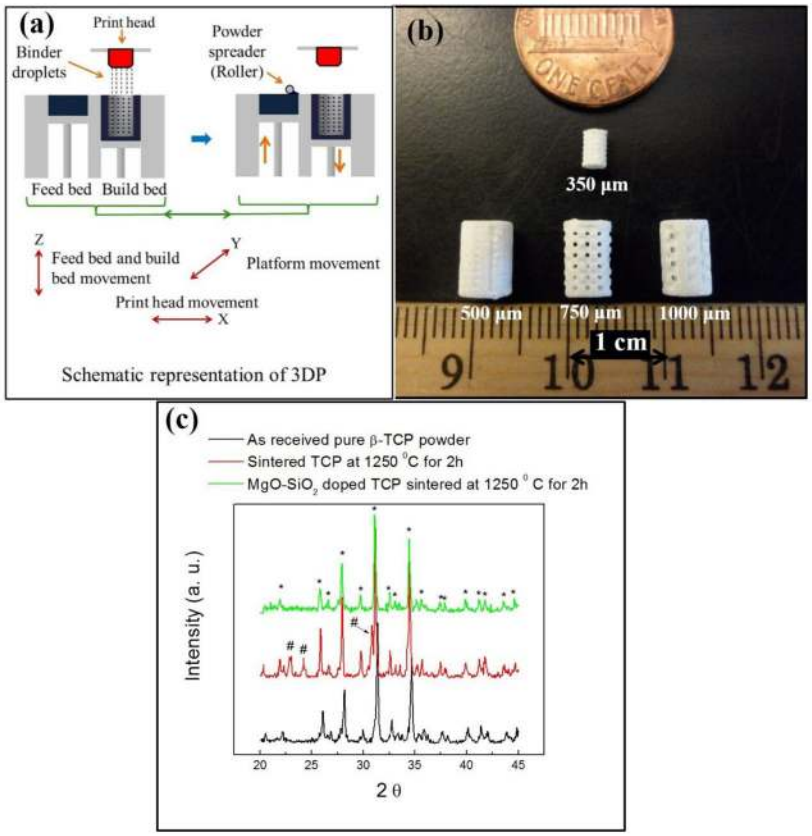

Figure 1.

(a) Schematic representation of the 3D printing (3DP); (b) Photograph of the MgO and SiO_2 doped TCP scaffolds. Smaller scaffolds with 350 µm designed pore size were used for rat model *in vivo*; (c) XRD patterns of 3DP pure TCP and Mg-Si doped TCP scaffolds.

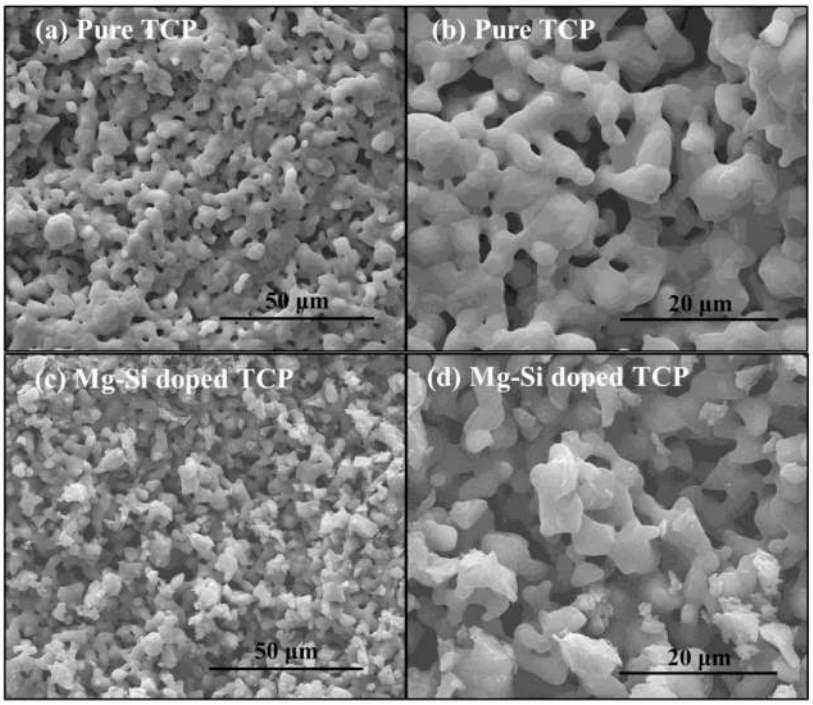

Figure 2.

Surface morphology of 3DP pure TCP and Mg-Si doped TCP sintered at 1250 °C: Pure TCP with low (a) and high (b) magnification, Mg-Si doped TCP with low (c) and high (d) magnification.

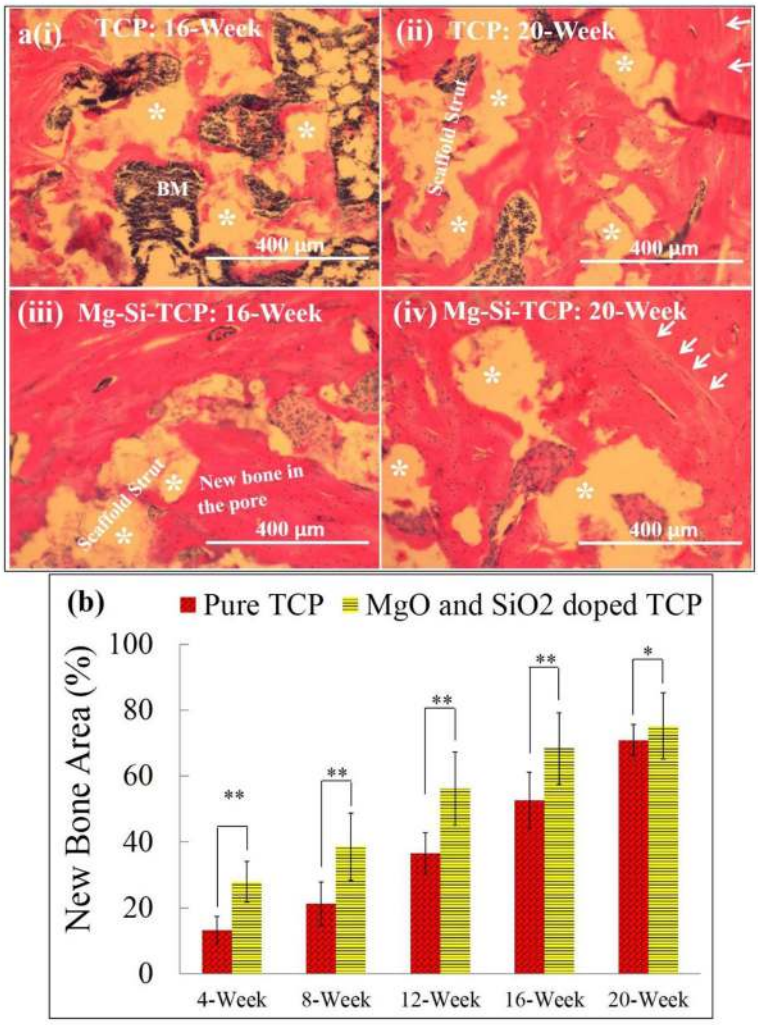

Figure 3.

(a) Photomicrograph of 3DP pure (i & ii) and Mg-Si doped TCP (iii & iv) scaffolds showing the development of new bone formation inside the interconnected macro pores of the 3DP scaffolds after 16 (i & iii) and 20 (ii & iv) weeks in rat distal femur model. Hematoxylin and Eosin (H&E) staining of transverse section. BM = Bone marrow; Arrows indicate the interface between scaffold and host bone; Star (*) indicates acellular regions derived from the scaffold. Color description: Black = Bone marrow; Pink/Reddish = New/old bone; Yellowish = acellular regions derive from scaffold; (b) Histomorphometric analysis of bone area fraction (total newly formed bone area/total area, %) from 800 μm width and 800 μm height H&E stained tissue sections (**$p < 0.05$, *$p > 0.05$, n=8).

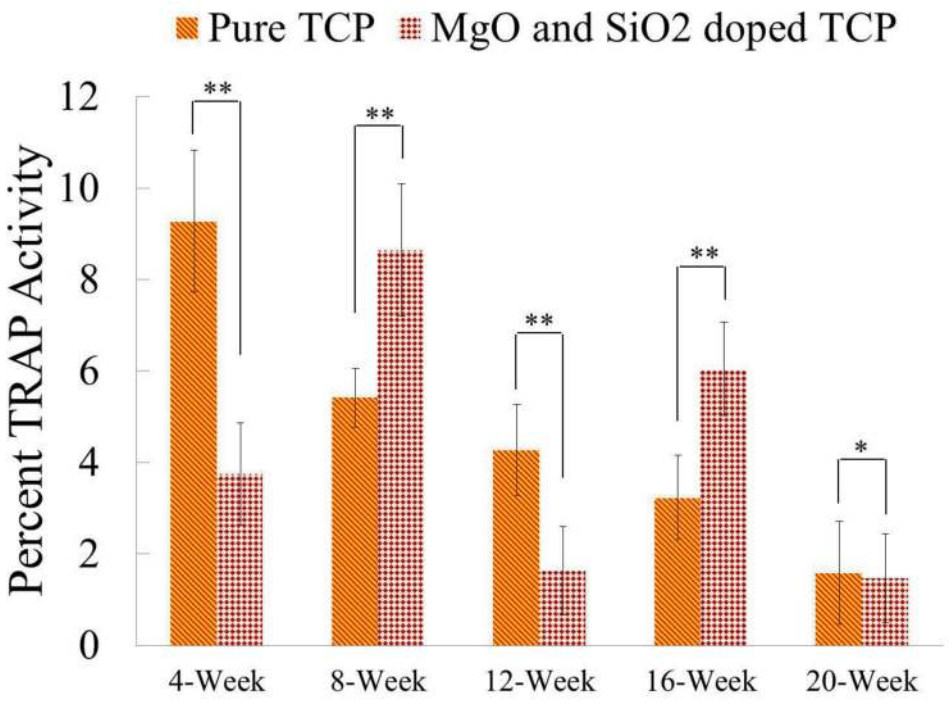

Figure 4.

Histomorphometric analysis of TRAP activity (TRAP positive area/total area, %) from 800 μm width and 800 μm height TRAP stained tissue sections (**$p < 0.05$, *$p > 0.05$, n=8).

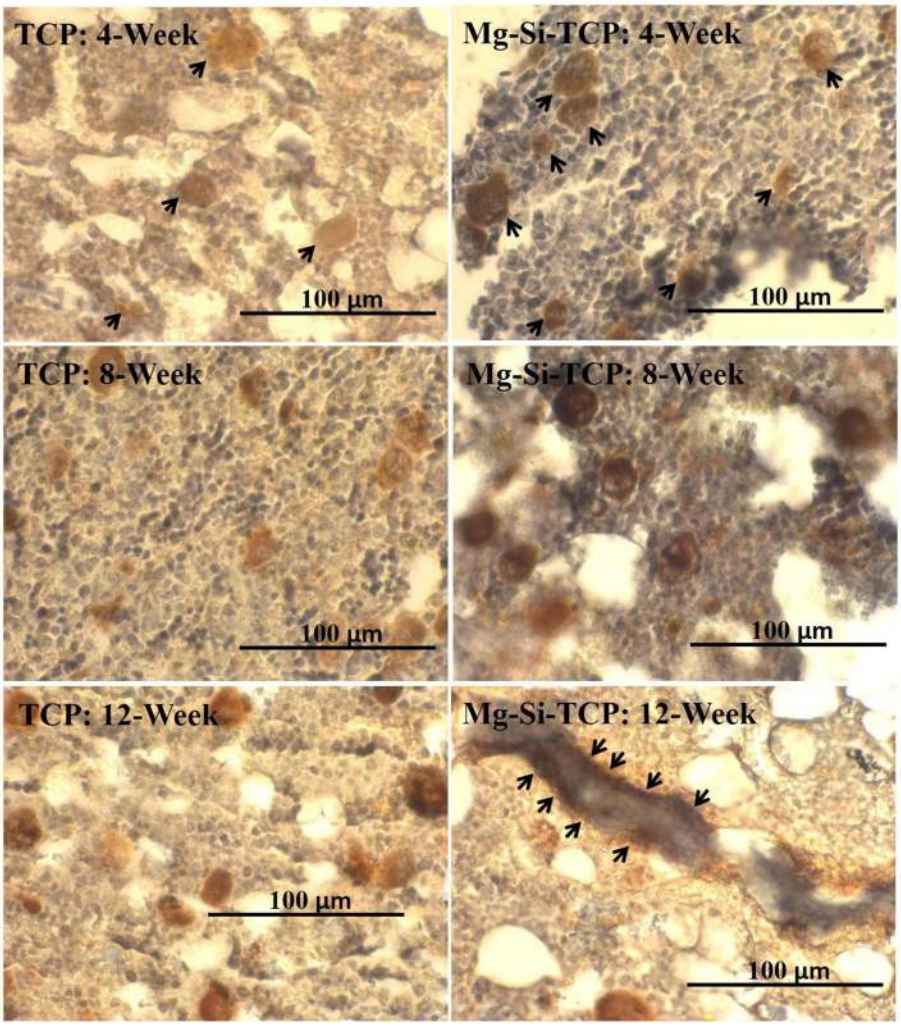

Figure 5.

Photomicrograph of vWF stained tissue sections showing blood vessel formation after 4, 8 and 12 weeks in 3DP pure TCP scaffolds and Mg-Si doped TCP scaffolds. Arrows indicate newly formed blood vessels inside scaffolds. vWF positive signals are brown with hematoxylin counterstaining.

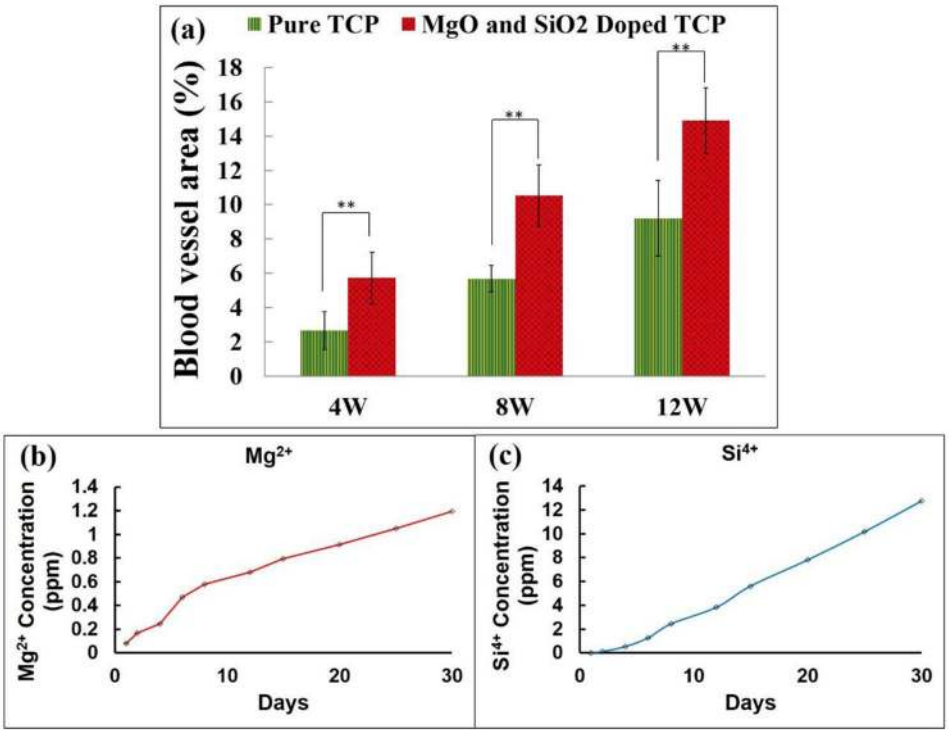

Figure 6.

(a) Histomorphometric analysis showing new blood vessel area comparisons between pure TCP and Mg-Si doped TCP (vWF positive area/total area, %) from 200 μm width and 200 μm height vWF stained tissue sections (**$p < 0.05$, *$p > 0.05$, n=8); Cumulative Mg^{2+} (b) and Si^{4+} (c) release in the phosphate buffer (pH 7.4) from Mg-Si doped 3DP TCP scaffolds.

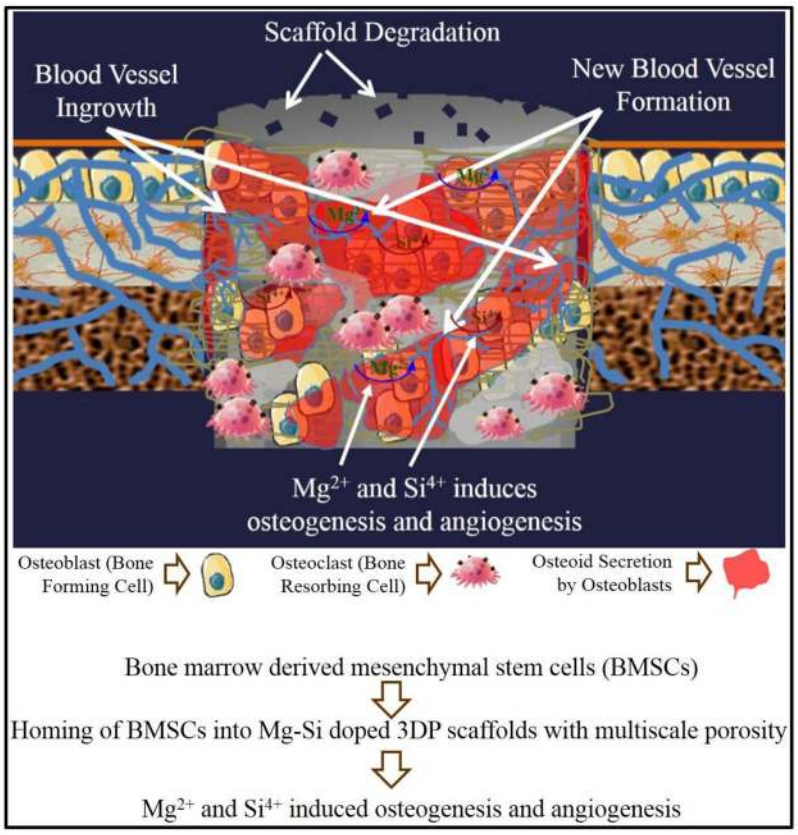

Figure 7.

Schematic representation showing accelerated osteogenesis and angiogenesis process triggered by Mg^{2+} and Si^{4+} ions from Mg-Si doped multiscale porous 3DP tricalcium phosphate tissue engineered scaffold when implanted on a defect site.

Table 1

Pore size, volume fraction porosity, and compressive strength of the Mg-Si doped 3DP TCP scaffolds.

Composition	3D interconnected designed pore Size (μm)	Sintered pore size (μm)	Designed macro porosity (%)	Total open porosity after sintering (%)	Compressive strength (Mpa) after Conventional Sintering at 1250 °C for 2h
Pure TCP [2]	500	421 ± 9.32	27	54.11 ± 3.97	6.62 ± 0.67
	750	662 ± 5.35	35	58.61 ± 5.35	4.37 ± 0.40
	1000	864 ± 4.10	41	58.22 ± 0.39	2.71 ± 0.67
Mg-Si doped TCP	500	394 ± 7.28	27	50.21 ± 5.37	6.79 ± 1.14 *
	750	603 ± 4.72	35	54.74 ± 2.88	4.47 ± 0.65 *
	1000	818 ± 6.65	41	56.69 ± 4.16	2.99 ± 0.73 *

* Statistically no significant difference between pure TCP and Mg-Si doped TCP